REPORT DOCUMENTATION PAGE	Form Approved OMB No. 0704-0188

The public reporting burden for this collection of information is estimated to average 1 hour per response, including the time for reviewing instructions, searching existing data sources, gathering and maintaining the data needed, and completing and reviewing the collection of information. Send comments regarding this burden estimate or any other aspect of this collection of information, including suggestions for reducing the burden, to Department of Defense, Washington Headquarters Services, Directorate for Information Operations and Reports (0704-0188), 1215 Jefferson Davis Highway, Suite 1204, Arlington, VA 22202-4302. Respondents should be aware that notwithstanding any other provision of law, no person shall be subject to any penalty for failing to comply with a collection of information if it does not display a currently valid OMB control number.
PLEASE DO NOT RETURN YOUR FORM TO THE ABOVE ADDRESS.

1. REPORT DATE *(DD-MM-YYYY)*	2. REPORT TYPE	3. DATES COVERED *(From - To)*
04-04-2007	Final Report	January 2004-January 2007

4. TITLE AND SUBTITLE

Synchrotron Based X-Ray Strain Mapping in Fatigued Materials Subjected to Overload

5a. CONTRACT NUMBER

5b. GRANT NUMBER
N00014-04-1-0194

5c. PROGRAM ELEMENT NUMBER

6. AUTHOR(S)

Thomas Tsakalakos (PI), Mark Croft (Co-PI)

5d. PROJECT NUMBER
07PR04210-00

5e. TASK NUMBER

5f. WORK UNIT NUMBER

7. PERFORMING ORGANIZATION NAME(S) AND ADDRESS(ES)

Rutgers, The State University of New Jersey
New Brunswick, NJ 08901

8. PERFORMING ORGANIZATION REPORT NUMBER

9. SPONSORING/MONITORING AGENCY NAME(S) AND ADDRESS(ES)

Office of Naval Research
495 Summer Street
Suite 627
Boston, MA 02210-2109

10. SPONSOR/MONITOR'S ACRONYM(S)
ONR

11. SPONSOR/MONITOR'S REPORT NUMBER(S)

12. DISTRIBUTION/AVAILABILITY STATEMENT

"Approved for Public Release; Distribution is unlimited".

13. SUPPLEMENTARY NOTES

14. ABSTRACT

Fatigue crack growth involves localized fracture at the crack tip, and it intrinsically depends upon the local internal strain/stress fields and accumulated damage in the vicinity of the tip. The purpose of this report is to directly correlate variations in crack growth rate with variations in the relevant local strains around the crack tip. The so-called "overload effect", namely the prominent crack growth rate retardation after a single overload cycle in an otherwise constant amplitude is studied. Our high spatial resolution measurements around fatigue crack are greatly facilitated by indexing our measurements to the fatigue crack itself. This crack based positioning is accomplished by measuring the beam intensity transmitted through the sample, with a transmission detector, so that a radiographic transmission profile can be constructed. Such transmission profiles enabled precise location of the crack and the crack tip in the x-ray beam.

15. SUBJECT TERMS

EDXRD, Strain Mapping, Fatigue

20070907331

16. SECURITY CLASSIFICATION OF:			17. LIMITATION OF ABSTRACT	18. NUMBER OF PAGES	19a. NAME OF RESPONSIBLE PERSON
a. REPORT	b. ABSTRACT	c. THIS PAGE			19b. TELEPHONE NUMBER *(Include area code)*

Contract Information

Contract Number	N00014-04-1-0194
Title of Research	Synchrotron Based X-Ray Strain Mapping in Fatigued Materials Subjected to Overloading
Principal Investigator	Thomas Tsakalakos (PI), Mark Croft (Co-PI)
Organization	Rutgers University, Materials Science and Engineering Dept., and Physics Dept.

Technical Section

Technical Objectives

The technical objectives of this contract where to use high energy, synchrotron based x-ray diffraction measurements to determine the local strain/stress fields in the vicinity of fatigue crack tips. These strain/stress field measurements were initiated to provide guidance for fundamental modeling of fatigue crack growth. Here it should be noted that such modeling is fundamentally grounded in these local strain/stress fields and that heretofore methods to actually measure these strain fields were essentially nonexistent. (The synchrotron based x-ray diffraction techniques used in this work or developed previously by our group under previous ONR contracts.) The specific focus of this phase of our research was the "overload effect" in which a single cycle overload, in an otherwise constant amplitude fatigued specimen, retards the crack growth rate for a certain number of cycles (or crack length) after the overload (this is described at greater length below). Understanding the overload effect is an important step toward developing models of variable amplitude fatigue loading such as are needed in reliable component life determination for Navy applications.

Technical Approach

In this section synchrotron based x-ray diffraction technical approach will be discussed. The discussion of the specific samples studied will be covered in the Progress section.

The application of synchrotron based energy dispersive X-ray diffraction (EDXRD) to a measurement of local strain fields in the vicinity of fatigue cracks was discussed in a previous article by the authors [1-2]. The technique exploits the high intensity/energy white beam (30-200 KeV) x-rays of the X17 wiggler beamline at the Brookhaven National Synchrotron Light Source (NSLS). A schematic of the experimental apparatus is shown in Figure T1. In EDXRD, the incident beam and detector remain fixed at the desired fixed scattering angle 2θ (with $2\theta=12^{\circ}$ in our experiments). A spectrum simultaneously spanning a set of Bragg diffraction lines is collected using a solid state Germanium detector. See Figure T2 for typical spectrum from one of the specimens studied under this contract.

The energy of a Bragg line, E_{hkl}, is related to the spacing, d_{hkl}, between of atomic planes in the material by the relation $E_{hkl}=6.199/[\sin(\theta)\, d_{hkl}]$ where $\{hkl\}$ are the Miller indices identifying the crystalline planes, E_{hkl} is in KeV and d_{hkl} is in Å. Fitting a given Bragg line allows the precision determination of its center of gravity (in energy) and the calculation of the d_{hkl} lattice plane spacing. Variations in the atomic plane spacing from position to position in a specimen are then determined from the shifts in d_{hkl}, as determined from the Bragg peak energy shift. In the strain variations reported here the shifts of the most

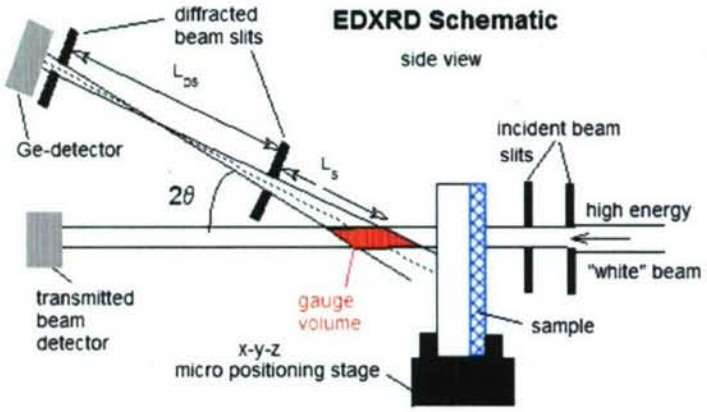

Figure T1 A schematic of the EDXRD experimental apparatus (X17B1 at NSLS) used in these experiments. The high-energy, "white" x-ray beam enters at right. The micro-swept through this scattering volume while the EDXRD spectra are collected by the energy-dispersive-Ge detector.

intense (h=3, k=2, l=1) line was used (see Figure T2). Using other Bragg lines, or a statistical average of a collection of Bragg lines, produce similar results. The strain variation from position to position in the sample is then determined from the shifts in Bragg peak energy via the relation $\varepsilon_{hkl}=(\Delta d/ d_0)_{hkl}=(\Delta E/ E_0)_{hkl}$ the a sample is translated through the beam. Here $\Delta d = d-d_0$ is the change in the lattice plane spacing, d_0 is the lattice spacing of the stress-free materials, $\Delta E = E_0 - E$ is the corresponding Bragg peak shift and E_0 is the center of gravity of peak of the stress-free material [1-2]. A point far from the crack tip was chosen to determine the E_0 value. An example of the magnitude of the Bragg line shift observed between positions in the specimens studied under this contract is shown in the inset a Figure T2. Measurements on Bragg lines with differing hkl yielded essentially identical results indicating that anisotropy's in the strain (i.e. variations in ε_{hkl} with differing hkl) is not crucial in the problem/material at hand and the hkl subscript is suppressed hereafter.

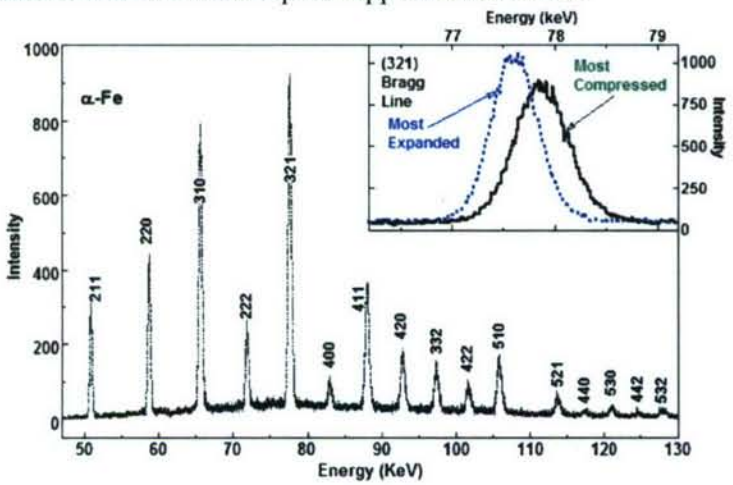

Figure T2. The EDXRD spectrum from the center of 4140 steel specimen which has been fatigued and subjected an overload cycle. The Miller indices of cubic α-Fe are shown. The Inset shows expanded views of the 321 Bragg lines, at two positions: the point in front of the crack tip, where the maximum tensile strain is observed: and the point at the center of the overload plastic zone where the maximum compressive strain is observed. The Bragg line shift to higher energy corresponds to a smaller lattice parameter.

The incident beam consists of highly parallel radiation and tightly collimated to a cross-section as small as 50μm X 50μm in our experiments near the crack tip (referrer back to Figure T1). Further from the tip where high-resolution is not crucial the slits were expanded to 100 μm parallel to the crack. The diffracted beam path was also highly collimated thereby defining a small gauge volume in the specimen over which the interatomic plane spacing was being measured. It is important to note that the stability of the rigidly fixed incident and scattering beam paths enables both high spatial resolution of the strain variation in the specimen and the high precision determination of the varying interatomic spacing ($\Delta d \sim \pm 0.0001$ Å).

A schematic of the compact tension (CT) geometry samples used in these experiments is shown in Figure T3. The coordinate system with the crack plane defined by y=0, the crack tip by x=0, and the

center of the fatigue specimen by z=0 is shown in the figure. The spatial volume studied was in a region approximately 300 μm (along the z-direction), in the crack plane (and less others otherwise specified) and approximately 50μm in height.

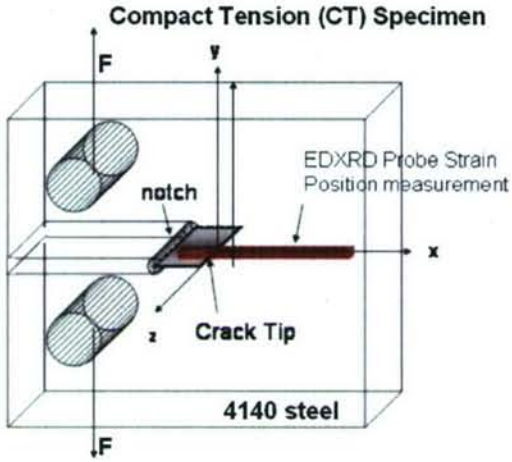

Figure T3. CT sample schematic, illustrating the location of the crack near the notch, and the position where the EDXRD measurement was performed.

It should also be noted that our high spatial resolution measurements around fatigue crack are greatly facilitated by indexing our measurements to the fatigue crack itself. This crack based positioning is accomplished by measuring the beam intensity transmitted through the sample (along the z-direction in the figure above), with a simple transmission detector, so that a radiographic transmission profile can be constructed. Such transmission profiles enabled precise location of the crack and the crack tip in the x-ray beam.

Since x-ray diffraction methods measure the inter-atomic spacings, our results are for the elastic strain only. In a sense the inter-atomic spacings can be thought of as imbedded local strain gauges which are "read" by x-ray diffraction. The presence of plasticity is evidenced by the local elastic strains in the absence of external load or the failure of the elastic strains to respond fully to an external applied load. Examples of both of these effects will be seen below.

Results

The discussion of our results achieved from this contract will be divided into three sections. The first deals with crack plane strain profiling, with in-situ loading cycle measurements. The second deals with out-of-plane 2D strain field mapping around the crack tip. Finally, the third section deals with the stress distributions within the crack plane.

Section P1: crack plane strain profiling with in-situ load cycles

Introduction

Attempts to quantitatively understand the growth rate of fatigue cracks, in response to cyclic loading, have a long history [3-5]. Since fatigue crack growth involves localized fracture at the crack tip, it intrinsically depends upon the local internal strain/stress fields and accumulated damage in the vicinity of the tip. The modeling work in this area has been carried forward with great resourcefulness despite the lack of clear, direct experimental data to provide fundamental guidance on these very local strain/stress fields. The purpose of this report is to directly correlate variations in crack growth rate with variations in the relevant local strains around the crack tip. The so-called "overload effect", namely the prominent crack growth rate retardation after a single overload cycle in an otherwise constant amplitude

fatigue experiment (see for example Figure P1.1a), will serve as a vehicle for this comparison [6-9]. Understanding the important "overload effect" is also a first step in the direction of eventual understanding of the fatigue crack growth under arbitrary variable amplitude loading conditions.

Our group has been involved in the ongoing development of high-energy synchrotron radiation x-ray diffraction techniques to map local strain fields in general [1], and in the vicinity of fatigue cracks in particular [2]. In this report we apply these techniques to a series of compact tension (CT) geometry 4140 steel test specimens which have been fatigued at constant amplitude, subjected to a single overload cycle and further fatigued to various distances (or times) beyond the overload point (see for example Figure P1.1b). The choices of samples and in-situ loading studies in this report were based upon the measured crack growth rate curve specific to our samples, shown in Figure P1.1a. For all of the samples high spatial resolution measurements of the systematic variation of the ε_{yy} strain component in the crack plane, along a line spanning the crack tip position have been made. Here, as in our previous work [2]: the external load is applied along the y-direction; the crack plane was defined by y=0; the crack tip is at x=0, unless otherwise noted here in; and all measurements are made over a small gauge volume in the center (defined by z=0) of the CT placket. It should be noted that as a result of our previous work we have substantially increased the spatial resolution of our strain measurements with the x-y cross-section of our gauge volume being routinely 50 μm X 50 μm in the vicinity of the crack tip. The data will show that such high-resolution is essential to reveal some of the fine structure details of the strain fields in the vicinity of the crack tip.

Fatigue damage occurs by definition under loading conditions. Importantly we have also measured ε_{yy} profiles with the CT samples under external (static) loads corresponding to various load levels in the constant amplitude, and overload, fatigue process. Specifically the changes in the strain profiles $\Delta\varepsilon_{yy}$ with changing load will be addressed here. This allows us to probe the crucial strain field response to these load levels before, during, after, and well-after the overload cycle. Mindful of the triaxial character of the stresses in these systems we will assume, for initial interpretation purposes, that the behavior of ε_{yy} and $\Delta\varepsilon_{yy}$ can be used as indicators of the behavior of σ_{yy} and $\Delta\sigma_{yy}$. Moreover, we assume, for the purpose of argument, that the extrapolation/evaluation of ε_{yy} and $\Delta\varepsilon_{yy}$ at the position of the crack tip can be used to suggest tentative qualitative arguments regarding the behavior of crucial crack growth parameters K_{max} and ΔK.

Experimental materials and preparation

The samples used in this study are 4 mm thick 4140 steel plackets fabricated in the compact tension (CT) geometry as described in reference 5. The fatigue preparations of the various samples are summarized schematically in Figure P1.1. All specimens specimens were first prepared under constant amplitude fatigue conditions with: K_{max}= 39.6 MPa $m^{1/2}$; and K_{min}= R K_{max} with R=0.1. At the crack length discussed here the applied load used to generate K_{max} was F_{max}=3.8kN. A test sample was then subjected to an overload with F_{OL}=2 F_{max} and was then fatigued at constant K= K_{max} while measuring the crack length, a by a potentiometric method (see Figure P1.1a for a schematic of this cycle sequence). The crack growth rate, da/dN (where N is the number of fatigue cycles) curve for this test sample is shown in Figure P1.1b. Here the constant crack growth rate before the overload has been used as a normalization factor. This da/dN curve shows the typical overload retardation affect [6-9]. This curve was used to estimate the crack lengths to which the cracks in subsequent samples should be grown in order to explore the strain fields at key points on the da/dN curve (see figure). A schematic of the samples prepared, and subsequent in situ loading experiments is shown in Figure P1.1a. The samples prepared were: a constant amplitude fatigue sample (denoted FS in the figure); a constant amplitude fatigue sample with a terminal overload cycle (denoted OL); and two samples which were fatigued, overloaded, and further fatigued to crack lengths appropriate for ~maximum da/dN retardation (denoted max-ret), and ~50% recovery to the pre-overload growth rate (denoted 50%-ret).

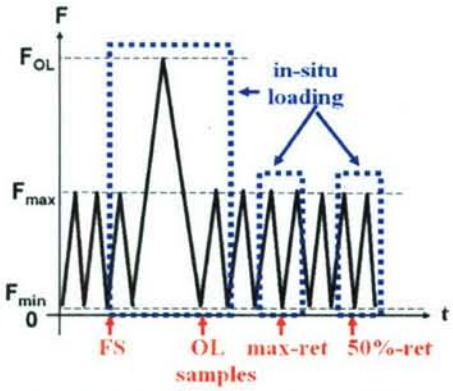

Figure P1.1a. A schematic of loading versus time for the constant amplitude fatigue, with embedded overload, experiments addressed in this report. The red arrows indicate the points where various samples were prepared by stopping in the fatigue sequence. The dotted rectangles indicate the regions in the fatigue process where in situ loading experiments were carried out. The max-ret and 50%-ret points occur respectively at ~$6(10)^3$ and ~$2(10)^4$ cycles beyond the overload point.

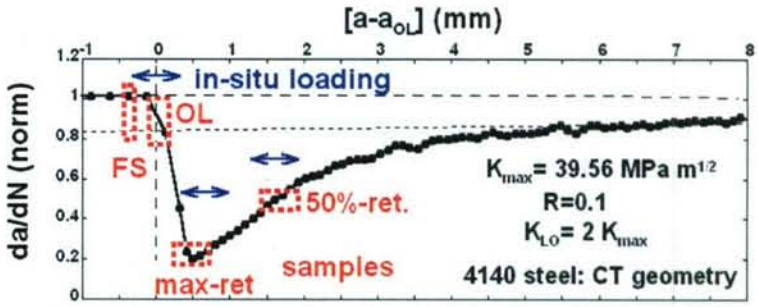

Figure P1.1b. The crack growth rate da/dN plotted versus crack length ,a, for one of our 4130 steel compact tension (CT) samples fatigued under constant amplitude conditions but with a single embedded overload cycle. The crack length is referenced with respect to the crack length at overload a_{OL}=25.4 mm and the curve has been normalized to the pre-overload crack growth rate of 2.05 $(10)^{-4}$ mm/cyle. Note the positions (dotted boxes) on the da/dN curve to which additional samples were prepared and the arrows indicating the regions where in situ load experiments were carried out.

Residual strains

Figure P1.2 shows high-resolution profiles of the residual (F=0, where F is the applied load) of the ε_{yy} strain component. These profiles are in the crack plane and along the crack propagation direction. The profile labeled FS and OL are respectively for a constant amplitude fatigued specimen and a similarly fatigued specimen with a F_{OL}= 2 F_{max} terminal overload applied. A series of points should be noted in these strain profiles.

The point labeled 1 in the figure lies in the wake-zone behind the crack tip. The presence of a narrow region adjoining the crack flanks where ε_{yy} manifested a sharp negative anomaly was noted in a previous work by the authors [2]. Subsequent work has clearly shown that this wake region is characterized by a strong anisotropy with ε_{xx} manifesting a sharp positive anomaly [10]. The region labeled 2 in the figure marks a positive upturn in ε_{yy} which is consistently observed upon approaching the crack tip from the crack (x<0) direction.

The features labeled 3 indicate the **process zone plastic region** in the vicinity of the crack tip. In the inset of Figure P1.2 an expanded view offers a better picture of the large-negative-peak strain anomaly characteristic of the process zone. In the constant amplitude fatigued case (FS): the crack tip is in just before the sharp drop in ε_{yy} which marks the entrance into the process zone; and the width of the process zone feature is approximately 0.15 mm (see figure inset). In the case of the overload sample (OL): the crack tip was determined to be in the center of the very large process zone feature; and the width of the process zone has expanded to about 0.6 mm.

The residual ε_{yy} strain profiles exhibit a positive maximum, labeled 4-FS and 4-OL for the constant amplitude and overload cases respectively. These points marked the furthest extent in front of the crack tip

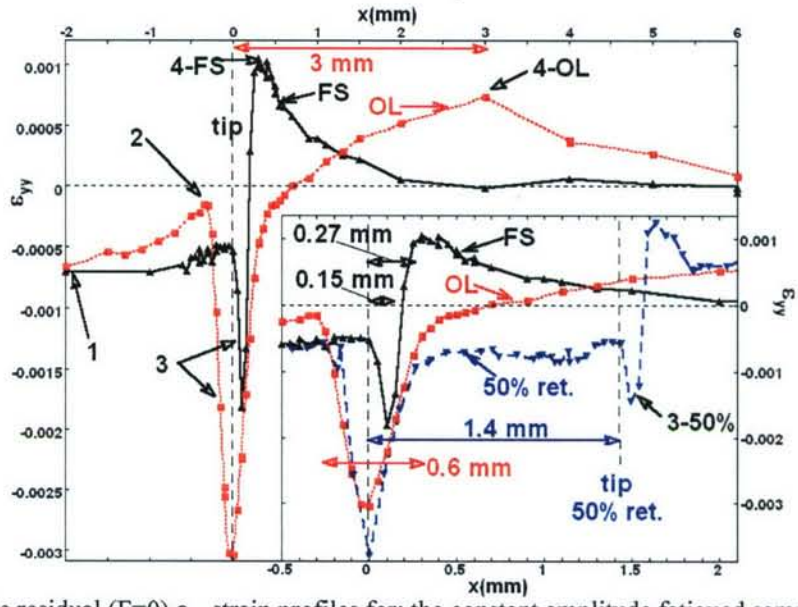

Figure P1.2. The residual (F=0) ε_{yy} strain profiles for; the constant amplitude fatigued sample (FS), the fatigued sample with an overload (OL) of magnitude $F_{OL}= 2\ F_{max}$, and the 50%-ret sample. The first two profiles are in the main part of the figure, and are shown again an expanded view in the inset with the the 50%-ret profile included. Unless otherwise stated in this and subsequent figures the following conventions are followed: the crack tip is at x=0 with the crack extending in the x<0 direction; and the strain profiles are along the crack propagation direction (x) and in the y=0, crack plane. In order to illustrate the movement of the crack tip through the OL induced strain field in this figure the 50%-ret strain profile has been displaced to align the OL feature at x=0 and the crack tip is at x=1.4 mm.

of the **monotonic plastic zone** and occur at distances of about 0.27 mm and 3.0 mm for the constant amplitude and overload cases respectively. It should be noted that the spatial extent of the monotonic plastic zone is approximately equal to the spatial extent of the overload crack growth retardation effect. This is consistent with long-standing notions that the retardation ceased as the crack tip exhibit the monotonic plastic zone [6-9]. Beyond the monotonic zone the residual strain is presumed elastic.

In the inset of Figure P1.2 we have also included the residual ε_{yy} strain profile for the post overload sample, whose crack growth rate has recovered to approximately 50% of the pre-overload rate (the 50%-ret sample). In this case (and in no other in this text) the crack tip position has been displaced to x~1.4 mm and the overload position has been aligned at x=0 to coincide with the original OL sample overload position. Interestingly the overload feature, for the 50%-ret sample, not just equal in strength but appears somewhat stronger than in the original OL sample. In view of the fact that these are different samples, and that the overload feature decreases rapidly in amplitude if one moves slightly away from the crack plane [2] the differences in the overload feature will be neglected here. The process zone feature for the50%-ret sample is (at x~1.5 mm, and labeled 3-50%) can be seen to closely resemble the feature for the constant amplitude case. This is consistent with the substantial recovery of the strain fields in the vicinity of the crack tip in this well after overload sample.

In-situ Load sequence through overload

Figure P1.3 shows the ε_{yy} strain profiles for a pre-fatigued sample cycled in situ through a fatigue cycle (between F=0 and F_{max}), an overload cycle (to $F= F_{OL}= 2\ F_{max}$), and a post overload cycle (between F=0 and F_{max}). The dwell times to collect the diffraction data at each of the points in the load cycle was

approximately 3 hours. The residual (F=0) strains profiles have been discussed at length above so we will concentrate on the under-load cases here.

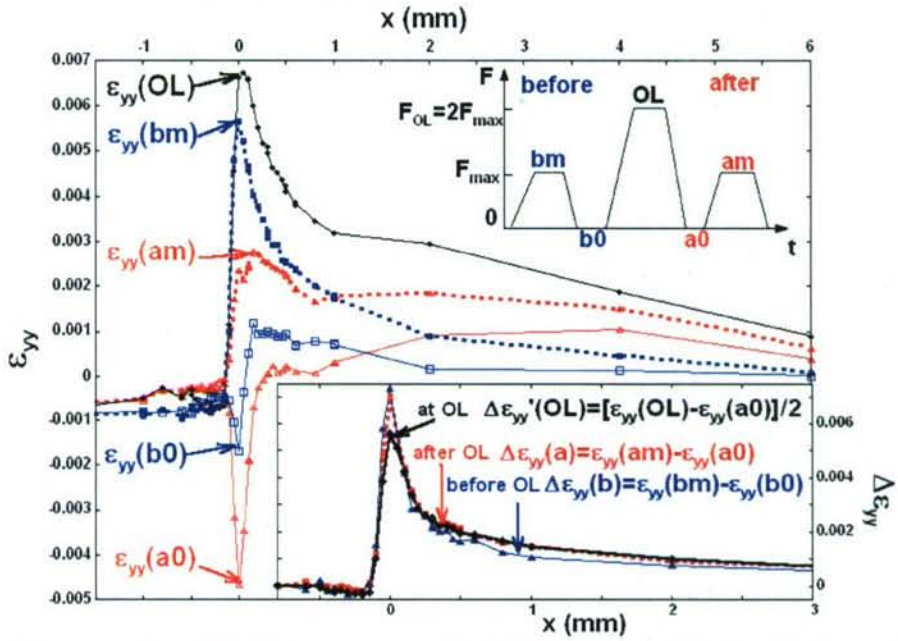

Figure P1.3. The ε_{yy} strain profiles for a constant amplitude fatigued sample before, during, and after an overload cycle. The load sequence (applied load, F, versus time, t) is illustrated in the upper inset schematic. The fact that this data was collected with statically applied loans has been emphasized in this schematic by the flat tops and bottoms on the sawtooth load curve. The strain profiles shown are for: the before overload $F=F_{max}$ (bm) and F=0 (b0) conditions; the after overload $F=F_{max}$ (am) and F=0 (a0) conditions; as well as the $F=F_{OL}= 2\ F_{max}$ (OL) condition.
Inset-lower) This inset shows a series of differential strains: $\Delta\varepsilon_{yy}= [\varepsilon_{yy}(\text{at } F= F_{max})-\varepsilon_{yy} (\text{at } F=0)]$ for both the before overload (b) and after overload (a) conditions; and the overload $\Delta\varepsilon_{yy}'(OL)= [\varepsilon_{yy}(\text{at } F= F_{OL})-\varepsilon_{yy} (\text{at } F=0 \text{ at a0})]/2$. In the case of $\Delta\varepsilon_{yy}'(OL)$ it should be noted that the differential strain has been divided by a factor of two because the applied load $F_{OL}=2\ F_{max}$ and it was desired to compare to the other differential strains obtained at the load of F_{max}.

Before discussing the under-load ε_{yy} profiles it is important to reiterate an assumption-for-initial-interpretation invoked in this report. Specifically we argue that the behavior of ε_{yy} (and $\Delta\varepsilon_{yy}$) can be used as an indicator of the behavior of σ_{yy} (and $\Delta\sigma_{yy}$). Moreover, we assume, for the purpose of argument, that the extrapolation/evaluation of ε_{yy} and $\Delta\varepsilon_{yy}$ to the position of the crack tip can be used to propose initial qualitative arguments regarding when the behavior of crucial crack growth parameters K_{max} and ΔK. With this in mind the observation that the magnitude of ε_{yy} at $F=F_{max}$ after the overload [ε_{yy}(am) in figure] is dramatically suppressed with respect to the ε_{yy} at $F=F_{max}$ before the overload [ε_{yy}(am) in figure] is particularly important. Namely it argues in favor of an **immediate suppression of the at-tip stress and the parameter K_{max} after the overload.** While the presence of the residual stresses after an overload has made this suppression of K_{max} expected on theoretical brown grounds our experimental results provided very real and direct support for it as well as an estimate of its relative magnitude.

Under load the ε_{yy} strain profiles for both the $F=F_{max}$ and $F= F_{OL}$ cases show large anomalies approaching the crack tip from the front (the positive x-direction). Under an external force the purely elastic stress component, σ_{yy}, manifests a $x^{-1/2}$ singularity approaching the crack tip from the front and its conjugate strain would be expected to reflect similar behavior. Of course residual stresses and/or plastic deformation will modify this singular behavior. In fact the residual stresses present before and after the applied load cause a very substantial deviation from the pure elastic singular behavior. As will be seen

below however the differential strain component, in which the residual strain is subtracted, does appear to manifest the singular functional form over a reasonable length scale.

Differential strain response before, after and during the overload

Since the crack tip growth driving force depends upon both K_{max} and ΔK [11] it is useful to consider also the quantitative load induced changes in the ε_{yy} profiles. Accordingly in the lower the inset in Figure P1.3 we show the difference profiles, $\Delta\varepsilon_{yy}$, obtained by subtracting the F=0 curve from the $F=F_{max}$ curves displayed in the main part of Figure P1.3. Both the before, $\Delta\varepsilon_{yy}(b)$, and after $\Delta\varepsilon_{yy}(a)$, overload differential strains are displayed. In addition a $\Delta\varepsilon_{yy}'(OL)$ curve is also shown in the inset of Figure P1.3. For $\Delta\varepsilon_{yy}'(OL)$ it was assumed that the residual strain, after the overload, was created by the overload application and that therefore $\Delta\varepsilon_{yy}'(OL)= [\varepsilon_{yy}(OL)- \varepsilon_{yy}(a0)]/2$. This is equivalent to treating the overload cycle ($F=F_{OL}$ to F=0) on the same basis as the constant amplitude ($F=F_{max}$ to F=0) cycles. The additional factor of ½ in the definition of $\Delta\varepsilon_{yy}'(OL)$ is to account for the fact that $F_{OL}=2F_{max}$ (rather than just F_{max}) for the purpose of comparing to the other $\Delta\varepsilon_{yy}$ curves obtained with $F=F_{max}$. Note that here, and in the data analysis below, spline fitting of the data to define a continuous function for subtraction purposes was used, when needed, for calculating differences in ε_{yy} profiles. All data points shown on the curves where actual data collection points of either (or both) the loaded or residual strain profile.

It is important to note that both the maximum amplitude and the overall x-dependence of the differential $\Delta\varepsilon_{yy}$ curves are almost identical before [$\Delta\varepsilon_{yy}(b)$] and after [$\Delta\varepsilon_{yy}(a)$] the overload cycle. Indeed, with the above defined normalization, the behavior of $\Delta\varepsilon_{yy}'(OL)$ closely resembles the other [$\Delta\varepsilon_{yy}$] curves except for some plasticity induced rounding of the peak at the crack tip position. Recall again the assumption that behavior $\Delta\varepsilon_{yy}$ provides an indicator of the behavior $\Delta\sigma_{yy}$ and therefore, at the tip position, of the ΔK fatigue parameter. Therefore given the fact that **$\Delta\varepsilon_{yy}$ is essentially unchanged by the imposition of the overload argues that ΔK is essentially unchanged immediately after the overload. As will be seen below $\Delta\varepsilon_{yy}$ is indeed suppressed some time after the overload and by inference a delay in and the suppression of ΔK after the overload is suggested.**

Singular behavior in the differential strain response

As alluded to earlier, purely elastic modeling predicts a $x^{-1/2}$ singularity in the stress, upon approaching the crack tip from the front. We have argued that evidence for such a singularity in the ε_{yy} strain would be expected however, residual strains/plasticity cause deviations from this behavior. By considering $\Delta\varepsilon_{yy}$ one subtracts off the residual strain and looks at just the material's local response to the impressed force. To test for singular behavior we follow a method similar to that used near singularities in thermodynamic phase transitions. For example plotting the inverse of the magnetic susceptibility versus temperature (T) above a ferromagnetic phase transition (at a temperature T_c) yields a linear Curie-Weiss behavior, reflecting the $1/(T-T_c)$ singularity (within mean field theory) in the susceptibility [12]. In the case at hand we will look for linear behavior, as x approaches zero (the crack tip), in $\Delta\varepsilon_{yy}^{-2}$ plotted versus x in order to test for $\sim x^{-1/2}$ type scaling.

Deviations from this elastic singular behavior are expected due to plasticity near the crack tip position however, the method of plotting used minimizes this effect. Moreover, two effects preclude looking for this singular behavior too far in front of the tip. Firstly in the compact tension (CT) geometry there is a node in σ_{yy} and consequently a linear far field strain, passing through zero, far in front of the tip. Secondly small variations in the choice of the zero stress inter-atomic lattice spacing, which are a negligible fraction of the in the large near-tip strains, could make large fractional contributions in the far field. Referring to the data in Figure P1.3, the strain field magnitude and nonlinear curvature appears to suggest singular behavior for x somewhere less than 2.5 mm.

Figure P1.4 shows $\Delta\varepsilon_{yy}^{-2}$ vs x plots for the three cases, plotted in Figure P1.3-inset; the before-OL [$\Delta\varepsilon_{yy}(bm)$] case, the before-OL [$\Delta\varepsilon_{yy}(am)$] case, and the at-OL [$\Delta\varepsilon_{yy}'(OL)$] case. In Figure P1.4 the $\Delta\varepsilon_{yy}^{-2}$

behavior both before (b) and after (a) the overload appears to manifest linear scaling with x (for x somewhat below 1.2 mm) as the crack tip is approached (see the dashed lines and the figure illustrating the scaling behavior). Despite the very large residual stress after the overload, the $\Delta\varepsilon_{yy}'(OL)^{-2}$ plot also manifests scaling behavior over a larger x-range (up to x~2mm). Interestingly the $\Delta\varepsilon_{yy}'(OL)^{-2}$ plot also superimposes with the $\Delta\varepsilon_{yy}(am)^{-2}$ as the crack tip is approached. This behavior is not surprising in view of the fact that the $\Delta\varepsilon_{yy}'(OL)$ and $\Delta\varepsilon_{yy}(am)$ curves in Figure P1.3-inset superimpose for wide ranges of x. Thus it appears that the elastic singular behavior approaching the crack tip from the front is reflected in the change in ε_{yy} induced by the applied external load.

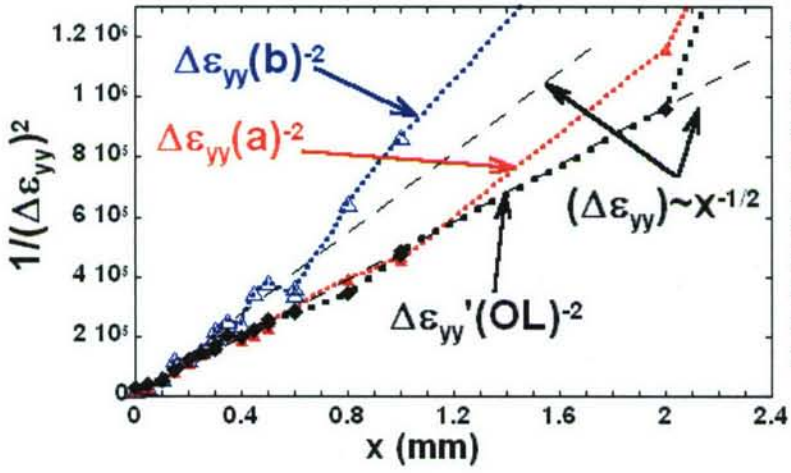

Figure P1.4. Plots of $1/\Delta\varepsilon_{yy}^2$, versus x in the region just in front of the crack tip where a square root singularity in the purely elastic behavior is anticipated. $\Delta\varepsilon_{yy}$= [ε_{yy}(at F= F_{max})-ε_{yy} (at F=0)] for both the before (b) and after (a) overload conditions. In addition the at-overload differential $1/\Delta\varepsilon_{yy}'(OL)^2$ is also plotted.

Maximum retardation sample strain response to load

In Figure P1.5 the ε_{yy} strain profiles for the max-ret sample for loads of F=0, F_{max}, and $F_{max}/2$ are shown. As expected the F_{max} profile manifests a large positive ε_{yy} peak at the crack tip. In contrast, the F=0 profile shows a strong negative peak at the position where the $2F_{max}$ overload (OL) was applied, with only a steep strain gradient type structure in the vicinity of the tip position. The intermediate load $F_{max}/2$ profile shows a dramatic decrease in the OL strain feature along with a more modest positive displacement (relative to the F=0 profile) in the tip region.

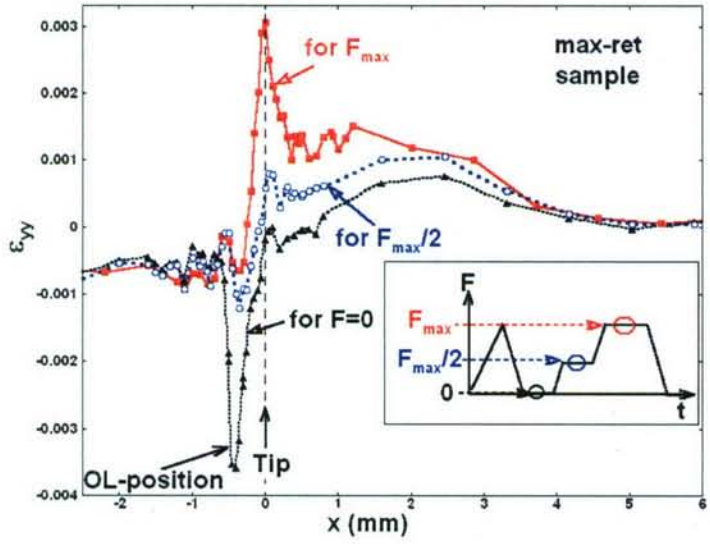

Figure P1.5. The ε_{yy} strain profiles for the max-ret sample for zero external load (F=0), for the maximum constant amplitude load fatigue load F_{max}, and for $F_{max}/2$. The positions at which the overload (OL) was applied and of the crack tip are indicated. The inset illustrates the load points in the fatigue cycle where the data was collected. Note that this data was collected with statically applied loans.

Differential strain response: maximum retardation sample

As noted above the crack tip growth driving force depends upon both K_{max} and ΔK, hence it is important to consider the quantitative load induced changes in the ε_{yy} profiles. Accordingly in Figure P1.6 we show the difference profiles, $\Delta\varepsilon_{yy}$, obtained by subtracting various curves in Figure P1.5. The"$\Delta\varepsilon_{yy}$ for ΔF_{tot}" curve representing the x-dependence of the differential shift in the ε_{yy} strain between F=0 and F=F_{max}. The $\Delta\varepsilon_{yy}$ for ΔF_{tot} curve very clearly manifests two strong positive peaks, one at the **overload x-position**, and one at the **crack tip x-position**. There is also a longer-range falloff in this differential strain in front of the crack tip.

With the data at hand and it is possible to breakdown the contributions to the differential strain response into contributions from a low applied force change, ΔF_{low} (from F=0 to F=F_{max}/2), and from a high applied force change, ΔF_{high} (from F= F_{max}/2 to F=F_{max}). The differential strain response in the low force region (see "$\Delta\varepsilon_{yy}$ for ΔF_{low}"in figure) shows a dramatic peak at the **overload x-position** with a longer-range falloff in the positive x-direction. In particular it should be noted that there is **no strong feature in the differential low force response at the crack tip x-position**. Interestingly the differential strain response in the high **force** region (see "$\Delta\varepsilon_{yy}$ for ΔF_{high}"in figure) shows a similarly dramatic peak but now located at the **x-position of the crack tip** with a longer range falloff beyond the tip. There is **no strong feature in the differential high force response at the overload x-position**. Thus our results support the notions: that between F=0 and F=F_{max}/2 the differential response is dominated by modifications in the OL spatial region; whereas between F= F_{max}/2 and F=F_{max} the differential response is dominated by modifications at the crack tip.

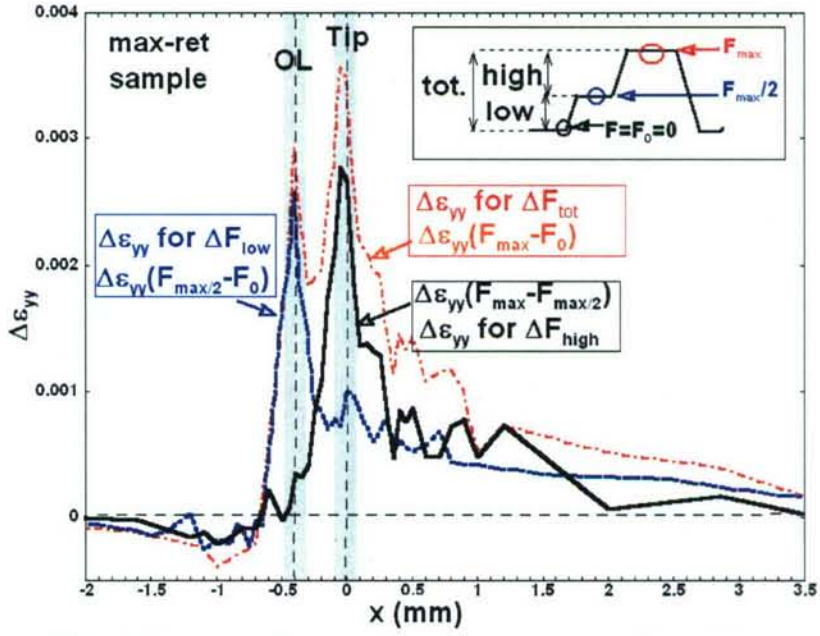

Figure P1.6. The "differential" strain profiles $\Delta\varepsilon_{yy}$ for the max-ret sample obtained by subtracting the ε_{yy} profiles at different loads shown in the previous figure. Specifically: for the "$\Delta\varepsilon_{yy}$ for ΔF_{tot}" case the F=0 curve was subtracted from the F=F_{max} curve; for the "$\Delta\varepsilon_{yy}$ for ΔF_{low}" case the F=0 curve was subtracted from the F=F_{max}/2 curve; and for the "$\Delta\varepsilon_{yy}$ for ΔF_{high}" case the F= F_{max}/2 curve was subtracted from the F=F_{max} curve

50% retardation sample strain and differential strain response to load

Figure P1.7 shows a plot of the ε_{yy} strain profiles for the 50%-ret. sample in the cases of zero load (F=0), and of F=F_{max}. In addition the differential strain, $\Delta\varepsilon_{yy}$, computed, as usual, by subtracting the F=0 profile from the F=F_{max} profile is shown. The overload feature at x~-1.4 mm is prominent in the residual (F=0) strain profile and is suppressed in the loaded F=F_{max} profile. Consequently the differential strain,

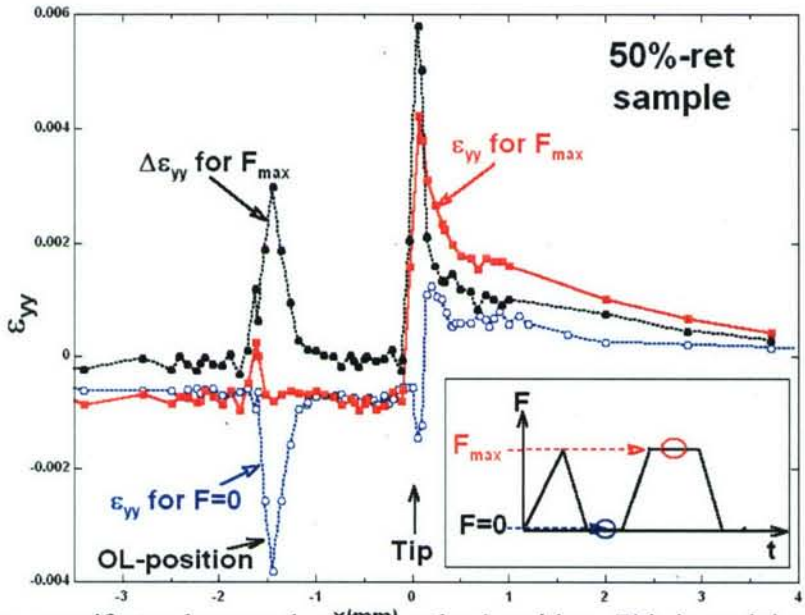

Figure P1.7. The ε_{yy} strain profiles for the 50%-ret. sample, for zero external load (F=0), and for F=F_{max}. Also shown is the "differential" strain profile $\Delta\varepsilon_{yy}$. The inset shows a schematic of the applied load, F, versus time, t, and identifies the load points where the data in the plot were collected.

$\Delta\varepsilon_{yy}$, manifests a large peak at the overload position. This is reminiscent of the behavior of the max-ret sample but with the overload feature now displaced the far enough from the tip feature to be totally resolved. It should be noted that the sharp structure in $\Delta\varepsilon_{yy}$ near x=-1.6 mm appears to result from experimental scatter amplified by subtracting the two curves.

Comparison of samples

We will now draw together and compare our strain profile results on the various samples under various load conditions. In Figure P1.8a we compare the ε_{yy} residual (F=0) strain profiles of the various pre-and post-overload samples studied here, with the convention that the crack tip occurs at x=0 (see dashed line in the figure). It should be noted that the overload strain feature is characterized by a large negative peak in ε_{yy} and that this feature moves from x=0 (for the immediately after overload curve), to x~-0.4 mm (for the max-ret curve), and to x~-1.4 mm (for the 50%-ret curve). This effect represents the stationary position of the overload with the crack tip propagating forward. The previously noted fact that, the process zone anomaly of the 50%-ret has almost recovered the same characteristic narrow negative anomaly in ε_{yy}, as is observed for the before-OL sample, is emphasized here by their superposition.

In figure P1.8b we plot together the ε_{yy} strain profiles under the load of F=F_{max} for the before-OL, after-OL, max-ret , and 50%-ret. samples/conditions. In addition ε_{yy} strain profile under the OL of F=F_{OL}=2F_{max}, is included for reference. The large suppression of the ε_{yy} strain from before to immediately after the overload is dramatically apparent in these curves. The slow recovery of the ε_{yy} strain upon moving from the after-OL, to the max-ret and still further to the 50%-ret conditions can also be seen. The values of these curves at the crack tip (i.e. x=0) should be noted for use below.

In Figure P1.8c we plot the $\Delta\varepsilon_{yy}$ differential strain profiles for the before-OL, after-OL, max-ret. , and 50%-ret samples/conditions. Several points should be noted here. First, there is essentially no change between the $\Delta\varepsilon_{yy}$ curves before and after the overload. Second, the max-ret $\Delta\varepsilon_{yy}$ curve is both

dramatically suppressed relative to the before-OL curve, and has a distinct bimodal peak structure. Moreover, one of the two peaks occurs at the crack tip position and the other at the overload position. Third, there is a recovery (near the crack tip position) in the 50%-ret $\Delta\varepsilon_{yy}$ curve in toward the behavior of the before-OL curve. Finally, the overload feature peak that was abutting the crack tip feature in the max-ret curve can be seen clearly resolved and to have moved to far behind the tip feature in the 50%-ret curve. Again the values of these curves at the crack tip (i.e. x=0) should be noted for use below.

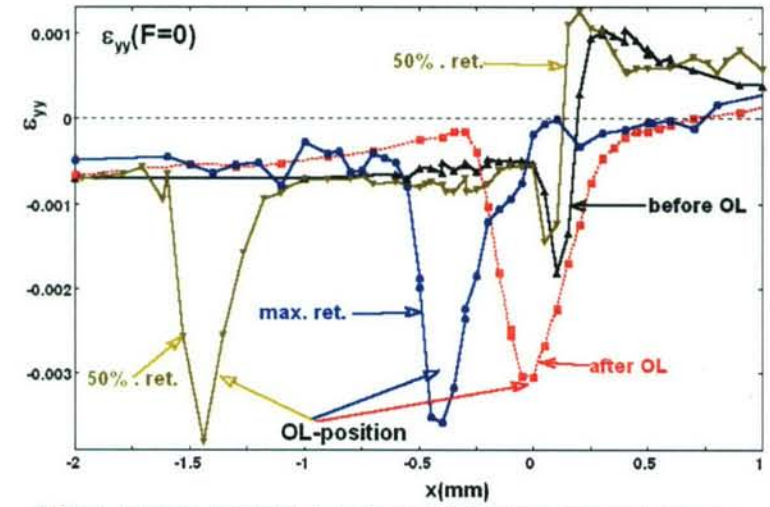

Figure P1.8a. A comparison of the ε_{yy} residual (F=0) strain profiles for the before-OL, after-OL, max-ret. , and 50%-ret. samples/conditions. The position of the OL feature can be seen to move progressively behind the propagating tip.

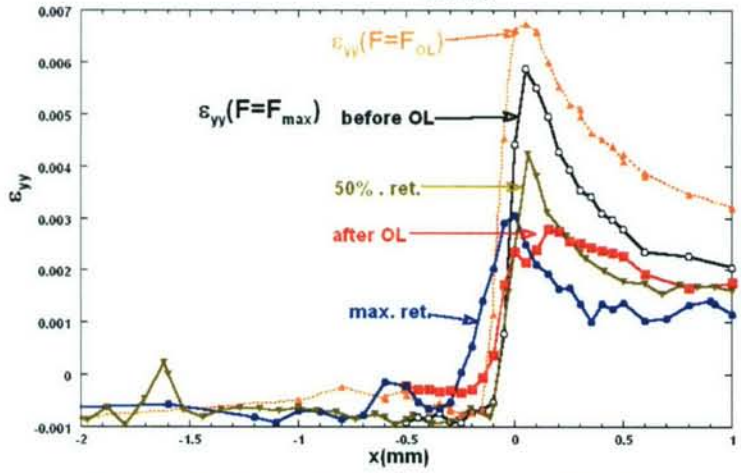

Figure P1.8b. A comparison of the ε_{yy} strain profiles under the load of F=F_{max} for the before-OL, after-OL, max-ret, and 50%-ret. samples/conditions. The ε_{yy} strain profile under the OL of F=F_{OL}=2F_{max} is included for reference. Note that the at-tip (x=0) values of these curves will be used in the discussion which follows.

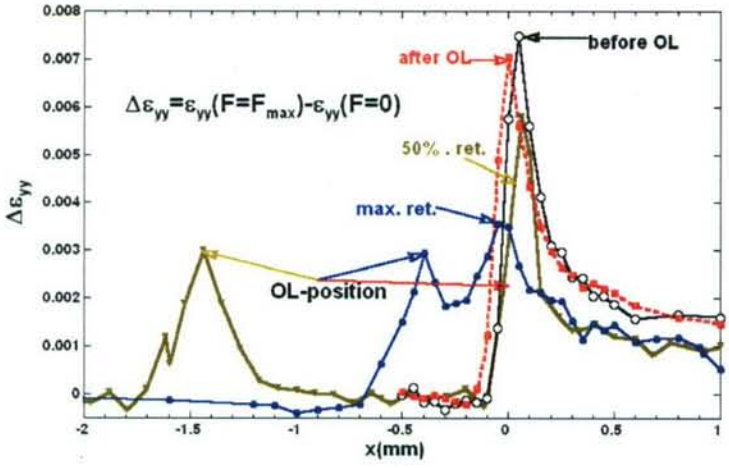

Figure P1.8c. A comparison of the $\Delta\varepsilon_{yy}$ differential strain profiles for the before-OL, after-OL, max-ret. , and 50%-ret. samples/conditions. Note that the at-tip (x=0) values of these curves will be used in the discussion which follows.

Since it is a conditions at the crack tip which enter models of the crack propagation rate, we plot in Figure P1.9 the values of $\varepsilon_{yy}(F=0)$, $\varepsilon_{yy}(F=Fmax)$, $\Delta\varepsilon_{yy}$ (F=0 to F=Fmax) obtained from the x=0 points of the previous three figures. For reference the single point at $\varepsilon_{yy}(F=F_{OL})$ is also ploted. The immediate suppression of $\varepsilon_{yy}(F=Fmax)$ by the overload with a slow recovery can be saying. The immediate introduction of a large negative strain after the overload in the residual $\varepsilon_{yy}(F=0)$ strain is clear along with the rather rapid recovery to nearer pre-overload levels. Finally the delay in the suppression of the $\Delta\varepsilon_{yy}$ (F=0 to F=Fmax) curve until the maximum retardation condition with a subsequent recovery should be noted. In order to compare fractional changes in these quantities we will, in what follows, normalize them to the values they had immediately before the overload.

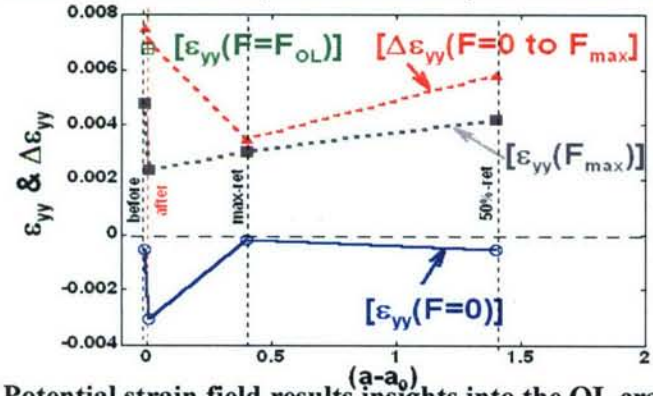

Figure P1.9. A summary of the **at-crack-tip values** of $\varepsilon_{yy}(F=0)$, $\varepsilon_{yy}(F=Fmax)$, $\Delta\varepsilon_{yy}$ (F=0 to F=Fmax), and $\varepsilon_{yy}(F=FOL)$ plotted versus crack tip position, measured relative to the overload. These values are taken from the x=0 values of the plots in Figures c1-c3.

Potential strain field results insights into the OL crack growth retardation effect

We now wish to summarize our strain field measurements in a way that might shed light on to the retardation of crack growth produced by the overload. Figure P1.10 shows an expanded plot of the normalized crack growth rate versus crack tip position shown in Figure P1.1b. This normalized curve makes the fractional magnitude of the OL retardation effect, compared to the constant amplitude rate, immediately visible. It should be noted that the crack growth rate OL effect in our case is not "ideal" in the sense that it does not quite recover to the pre-overload rate far beyond the overload point. This experimental effect is not on common will not be addressed here.

Figure P1.9 in the previous section displayed the experimental values of ε_{yy}(at $F=F_{max}$) and $\Delta\varepsilon_{yy}$(between F=0 and $F=F_{max}$) at the position of the crack tip plotted versus the crack length, relative to the overload position (as measured both from the strain field data and by microscopy). The values of these crack tip strains have been normalized to their values before the overload point in order to provide the fractional changes in the strain parameters, as a function of proximity to the overload position. Can be plotted and compared to the crack growth retardation effect. The data for the normalized values of ε_{yy}(at $F=F_{max}$) {labeled $[\varepsilon_{yy}(F_{max})]_{norm}$ in the figure}, and $\Delta\varepsilon_{yy}$(between F=0 and $F=F_{max}$) {labeled $[\Delta\varepsilon_{yy}]_{norm}$ in the figure}at various crack lengths are superimposed with the normalized da/dN curve plotted in Figure P1.10.

For the purpose of discussion we will follow the proposal of Noroozi et al. [4] who characterized the crack growth rate driving force with the expression $da/dN\alpha\ [(K_{max})^{1-p}(\Delta K)^{p}]^{\gamma}$. For 4140 steel specimens studied here the estimated of p=0.83 and γ=3 have been made [13]. Our experiments have of course measured only the local strains. As noted above we must again rely on the assumption that behavior of ε_{yy} and $\Delta\varepsilon_{yy}$ are a valid indicators of σ_{yy} and $\Delta\sigma_{yy}$ and therefore when evaluated at the tip position of the crucial parameters K_{max} and ΔK. Proceeding on this assumption a series of observations and inferences can be made.

Referring to Figure P1.10 the most striking correlation is that between the position and magnitude of the overload induced anomaly in da/dN and the magnitude and position of the dip in the $[\Delta\varepsilon_{yy}]_{norm}$ points. This strongly supports the dominant contribution of the $(\Delta K)^{p}$ to the overload retardation effect. Moreover, noting that $[\Delta\varepsilon_{yy}]_{norm}$ was essentially unchanged immediately after the

overload and manifests a delayed depression, reinforces the correlation with the delay in the overload da/dN retardation effect. The inference

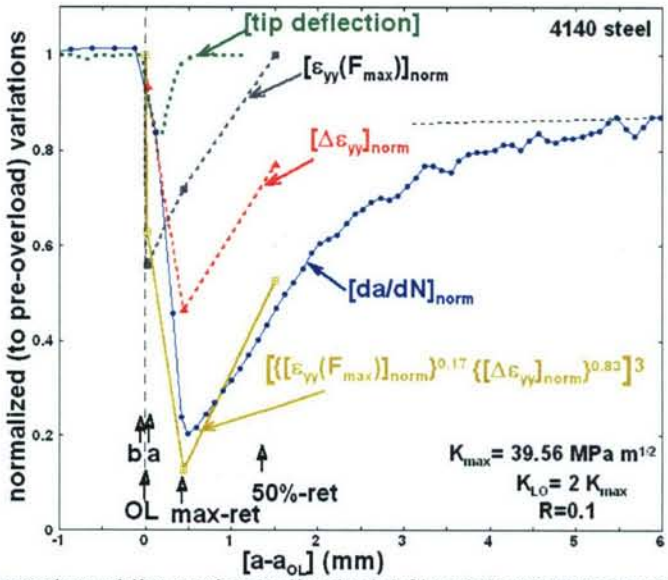

Figure P1.10. A superposition of the crack growth rate da/aN and the at-crack-tip values of $\varepsilon_{yy}(F_{max})$, and of the differential strain $\Delta\varepsilon_{yy}$. The values for these parameters are plotted for the before-OL (b), after-OL (a), max-ret , and 50%-ret. samples/conditions . The abscissa is the crack length referenced with respect to the overload point. All of the ordinate values have been normalized to those just before the overload so that fractional changes can be compared (hence the label norm applied to all of the variables). For completeness the crack retardation expected from observed tip path deflection has also been included (this effect will be discussed in a separate publication). Also plotted is the expression model expression $[\{[\varepsilon_{yy}(F_{max})]_{norm}\}^{1-p}\{[\Delta\varepsilon_{yy}]_{norm}\}^{p}]^{\gamma}$ with p=0.83 and γ=3.

here is that the delay in the suppression of ΔK leads, but the driving force, to the delay in the overload da/dN anomaly. Similarly, the fact that $[\varepsilon_{yy}(F_{max})]_{norm}$ is immediately depressed after the overload, whereas the da/dN anomaly onsets more slowly, is consistent with the minor role that the $(K_{max})^{1-p}$ plays in the crack growth driving force.

Encouraged by these qualitative correlations it is worthwhile taking the comparison one step further by comparing the full expression $[\{[\varepsilon_{yy}(F_{max})]_{norm}\}^{1-p}\{[\Delta\varepsilon_{yy}]_{norm}\}^{p}]^{\gamma}$, with p=0.83 and γ=3, to the $[da/dN]_{norm}$ in Figure P1.10. The overall striking agreement between this trial expression and the crack growth rate behavior is probably fortuitously good in view of the assumptions made and the limitations of the experimental data. Nevertheless, pending continued critical model assessment and more detailed experimental work the agreement appears highly supportive of the fundamental modeling methods being applied by G. Glinka and coworkers.

Section P2: residual stress strain field mapping

Introduction

The importance of **actually measuring** the local strain/stress fields around a crack tip upon which models for crack growth are built was noted above. The role of understanding individual fatigue cycle excursions, like the overload effect, in developing models for crack growth under variable amplitude fatigue loading was also noted. The work summarized above concentrated upon variations in the in-crack-plane strain variations. We have also been concerned with mapping the out-of-plane

variations in the strain fields around crack tips. In this section we will summarize some of our 2D strain field mapping results for the case of 4140 steel specimen with a single overload cycle.

The samples used in this study were 4 mm thick 4140 normalized alloy steel plackets in the single edge notched tensile (SET) geometry [2]. The constant amplitude fatigue cracking was performed with sine-wave loading at 10 Hz, with a peak stress intensity Kmax of 49.8 MPa-$\sqrt{m}$, at a load ratio R = Kmin/Kmax = 0.1. Overload cycles were at an overload ratio (OLR) of 2; i.e., to a peak load of 99.6 MPa-$\sqrt{m}$. Fatigue cracks in the samples were grown up to the sample-midline with the crack tip lying along a line between the centers of the loading pins. The coordinate system has been chosen with: the z=0 plane lying at the center of the sample (2 mm from each surface); the crack plane being defined by y=0; and the x=0 being located at the crack-tip (here the crack lies along x<0 and the propagation is in the +x direction) [2]. It should be noted that all of the x-ray strain results discussed herein are centered on the z=0 central plane of the specimens.

Our previous work has shown a systematic fall off in the crack plane strain anomalies as one moves off of the crack plane [2]. These results motivated higher resolution studies, of ε_{yy} profiles perpendicularly crossing the crack plane of the fatigue overloaded (FO) specimen, illustrated in Figure P2.1. In Figure P2.1a the x=-2 profile (with the 1 and 2 strain features identified above) is included to compare the at-crack wake anomaly well behind the tip, to the much larger effects near the crack tip [2,10]. In the x=-0.6 profile a smaller version of this negative dip in ε_{yy} now appears to ride on an increasing negative background that is growing as the crack tip plastic zone is approached. This background takes the form of a broad (extending ~2 mm from the crack plane) negative enhancement of a ε_{yy} (see 3 in figure). There is a qualitative change in behavior by x=-0.4, where a positive tending local peak in ε_{yy} has begun to develop (the onset of the α-structure discussed below) superimposed on the overall broad and increasing negative enhancement of ε_{yy} approaching the tip. Indeed, Figure P2.1a is dominated by the dramatic compressive effect at the epicenter of the overload plastic compressive zone in the x=0 profile (see 4 in figure). Perhaps equally as dramatic however is the sharp structure occurring immediately behind the tip as illustrated in the x=-δ (0<δ <0.2 mm) and x=-0.2 mm profiles. [Here the x=-δ positional uncertainty arises due to data collection in a separate beam time.] It is apparent from the figure that a sharp (within $\pm$ 0.15 mm of the crack plane) positive-tending local peak in ε_{yy} appears immediately behind the tip. This peak (labeled α in the figure) rides on the larger, longer-ranged plastic compressive zone background, causing dual negative strain peaks,(see 3 in the figure) on either side of the local α-tensile peak. It is worth noting that the local α-tensile deviation is reflected in the y=0, crack plane profile for fatigued-overloaded specimens in general (see for example the point labeled 2 in figure P1.2).

In Figure P2.1b the ε_{yy} strain profiles, transverse to the crack plane, at x=+0.2 and 0.4 mm (in front of the tip) are shown for the FO specimen. Both of these profiles are topographically similar to those observed immediately behind the tip; a central positive-tending peak (labeled β in the figure) riding on a compressive (negative) background leading to broad negative peaks (labeled 5 in the figure) on either side of the crack plane. The β-tensile dip the in the x=+0.2 and 0.4 mm profiles corresponds to the appearance of a tensile tendency of the strain in the crack plane in front of the tip. In the x=+0.4 mm profile the compressive lobs have become smaller in magnitude and strain at the β-tensile peak reaches an absolute positive values at its peak (at y=0).

The high spatial resolution strain profiles in Figure P2.1 (along with others not shown) have been interpolated into the higher resolution contour plot of the crack tip region for the FO sample shown in Figure P2.2. The at-crack (or wake) ε_{yy}-anomaly (labeled C/1) can be seen extending along the crack entering the figure from the left has been noted previously by the authors in reference [2]. The regions of positive ε_{yy} values, bordering the crack at a distance of ~0.5 mm from the crack, are labeled D/2. The very sharp epicenter of compression at the tip is noted and the wide extension of the negative-ε_{yy} region extending vertically from the tip is clear from the figure. The β-type tensile dip, extending toward the tip

from the front, is very articulated. Finally the dramatic positive peak α-feature appears as a sharp island interposed between the C/1-structure along the crack and the large compression at the tip. The spatial extent and positioning of the α-type tensile dip suggest that it is related to the constant amplitude process

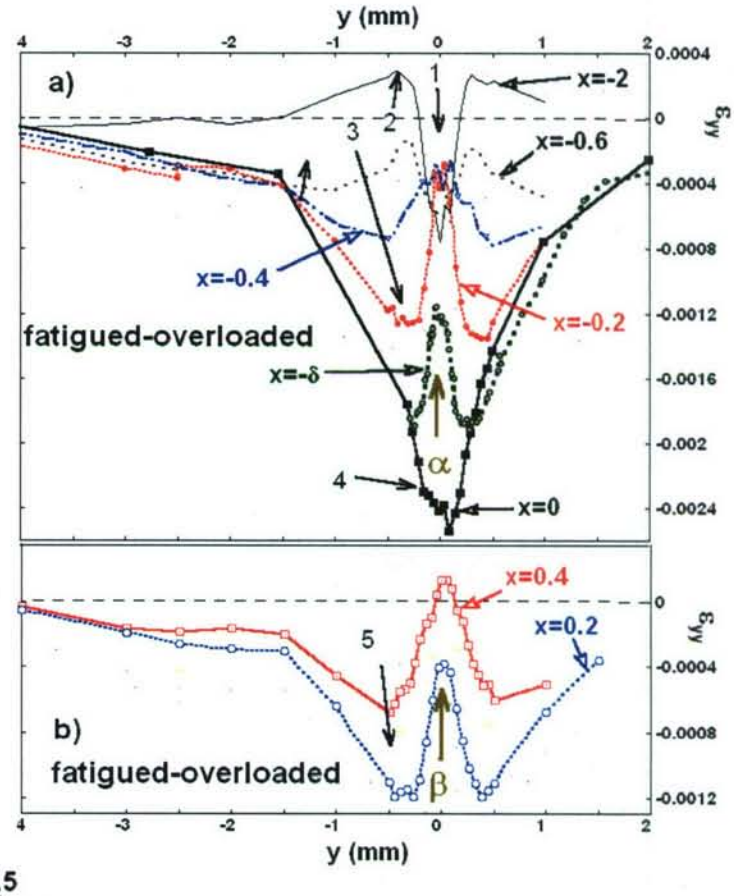

Figure P2.1. ε_{yy} strain profiles traversing the crack plane (along the y-direction) of the FO specimen at various positions (x) with respect to the crack tip. a) Profiles in the range – 2 mm ≤ x ≤ 0.0 mm.
b) Profiles in the range 0.2 mm ≤ x ≤ 0.4 mm.

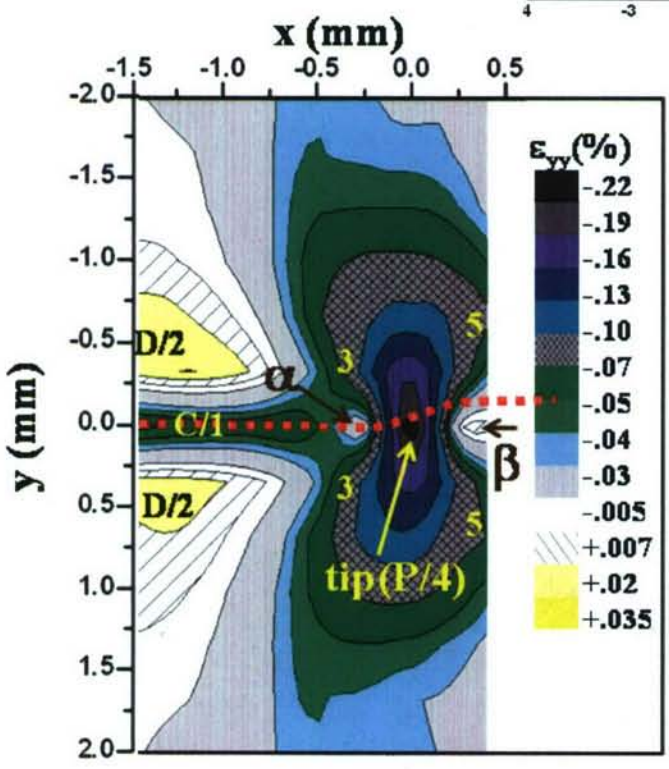

Figure P2.2. A higher spatial resolution contour plot of the ε_{yy} strain component near the crack tip of the FO specimen.

zone which created the wake-effect but which has been modified by the imposition of the large compressive stress of the overload plastic zone.

Optical Surface Height Mapping Measurements

It is instructive to make a direct correlation between surface observations of crack growth and the overload strain field map in Figure P2.2. Our group has studied multiple overloaded samples of both the single edge notch tensile (SET) and in the compact tension (CT) [2] geometry. In all of these materials a transient deflection in the crack tip propagation was observed at the overload point. Quantification of this deflection was made by digitizing optical microscopy photographs. These deflections are always of comparable magnitudes in the similarly loaded materials. The surfaces of the (CT) geometry specimens had been polished previous to the fatigue experiments and allowed detailed white light interference surface height mapping. Note that the the fatigue parameters for these 4140 steal CT geometry samples were K_{max}= 39.6 MPa $m^{1/2}$; K_{min}= R K_{max} with R=0.1, and with the overload cycle having K_{OL}= 2 K_{max}.

Figure P2.3. shows a surface height mapping of a specimen that was fatigued at constant amplitude, given a single overload cycle and removed from the fatigue apparatus. (These optical surface height profiling measurements were performed using a Zygo Inc. New View 5200 optical profiler. Discussion of white light optical surface profiling can be found in reference [16].) The blue regions in the figure are the most deeply depressed and the red regions are the highest. Moreover, the 3-D perspective is also used in the display of the data. A "valley" of depression indicates the wake zone path of the crack under the constant amplitude fatigue. The large "bowl-like" depression at the end of this valley is the surface deformation caused by the overload.

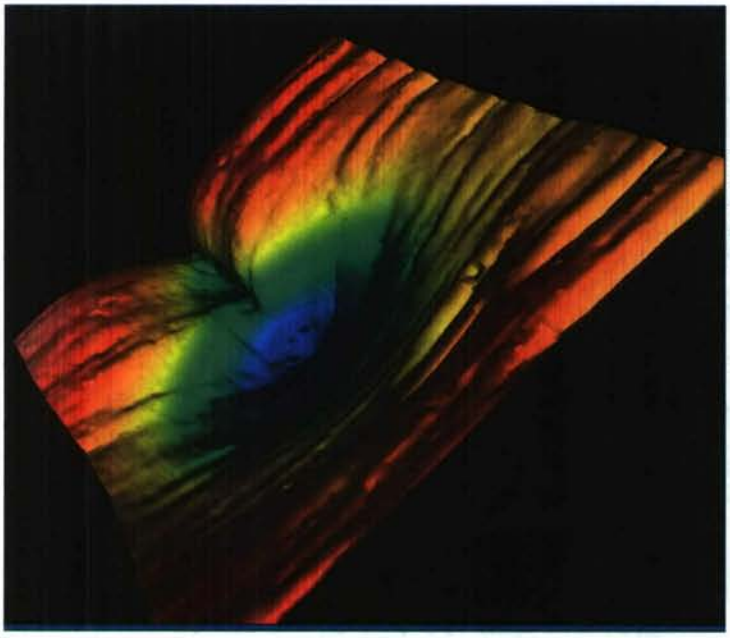

Figure P2.3 3D perspective surface topological map of the surface height for a 4140 steel specimen fatigue a constant amplitude with a terminal overload cycle.

Figure P2.4 shows a surface height mapping of a specimen that was fatigued at constant amplitude, given a single overload cycle and subsequently fatigued well beyond the overload point. Figure P2.4a shows the optical image of the crack path in which the overload deflection effect is abundantly clear. Figure P2.4b shows the perspective surface height map from the same data set. The vestiges of the overload depression are clear and the crack tip growth deflection at the beginning of the overload region can be seen. In order to quantify the magnitude of the surface height changes Figure

P2..4c shows a series of linear surface height profiles extracted along various paths (labeled 1-5) from the surface height map in Figure P2.4b.

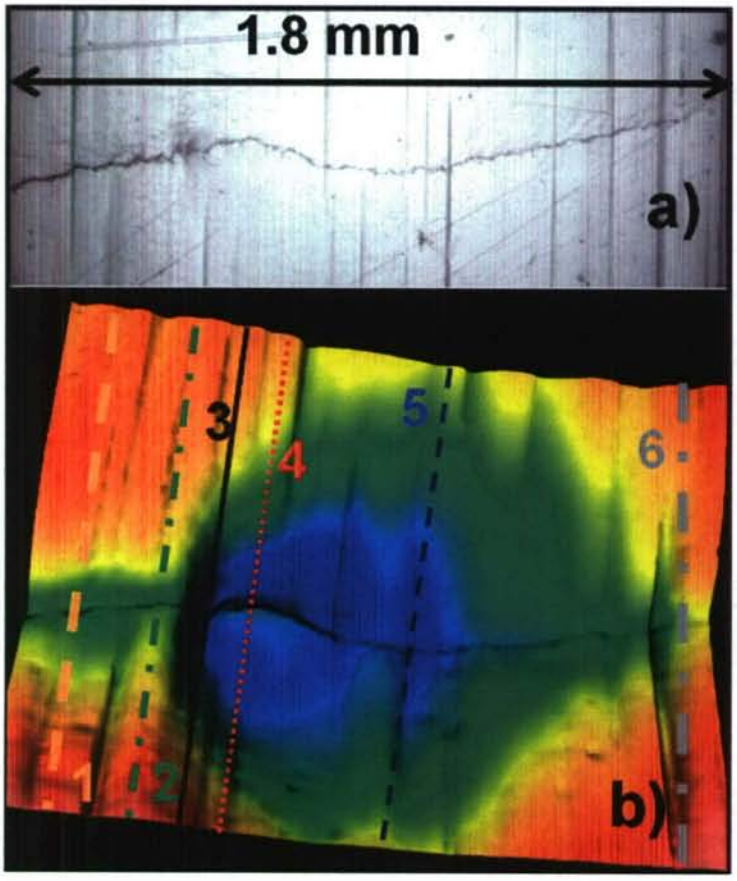

Figure P2.4a The optical image of the surface of a 4140 steel specimen fatigue a constant amplitude subjected to a single overload cycle and subsequently fatigued well beyond the overlooked point. The deflection in the path of the crack tip propagation due to the overload should be noted.

Figure P2.4b The 3D perspective of the surface topological map from the same data set shown in a) above. The correlation of the crack propagation deflection with the overload depression should be noted. Plots of the height along the paths labeled 1-5 are shown and the figure below.

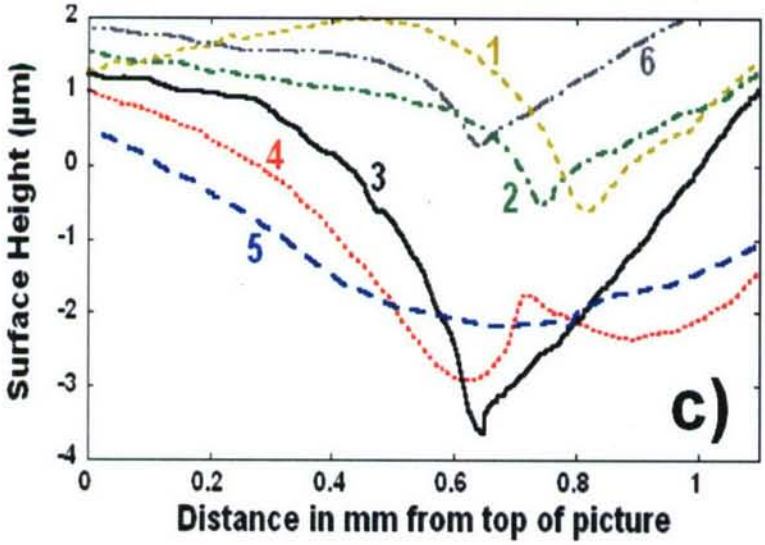

Figure P2.4c The linear plots of the surface height versus position on the lines labeled 1-5 in the figure b) above.

Conclusion

The selected results presented here provide a detailed picture of a fatigue crack strain field above and below the crack plane after an overload cycle. These results, along with others in this ongoing study, yield actual microscopic strain field profiles to compare in detail with theoretical models. The wealth of structure in these strain field mappings will provide important grounding for theoretical and modeling studies.

Finally, the surface measurements of the crack growth (immediately above) can be correlated to the overload strain field map in Figure P2.2. Overlaying the crack propagation trajectory (see red rotted line in Figure P2.2) of an identically fatigued-overloaded sample which was subsequently fatigued through the overload region one can see a clear trajectory displacement when propagating through the overload strain field. The observation of similar trajectory deviations in the overload region appears to be a common feature in such heavily overloaded specimens studied thus far by our group and suggests that the deviation arises in order to avoid the heavily compressed central region of the overload strain field. Of course a bifurcation of alternative trajectory deviations must occur with the experimental details dictating which path around the central overload compression is taken.

Section P3: stress distribution

Our EDXRD method measures only the local strain distribution. However we since we have measured both the ε_{yy} and ε_{xx} strain profiles, in the crack plane, for our fatigued overloaded CT specimen we are in a position to evaluate the residual stress components within the expected plane strain approximation. Accordingly in figure P3 .1 we show the variation of the σ_{yy} and σ_{xx} stress components of the residual stress distribution for a fatigued overloaded sample (see figure four the fatigue and overload values).

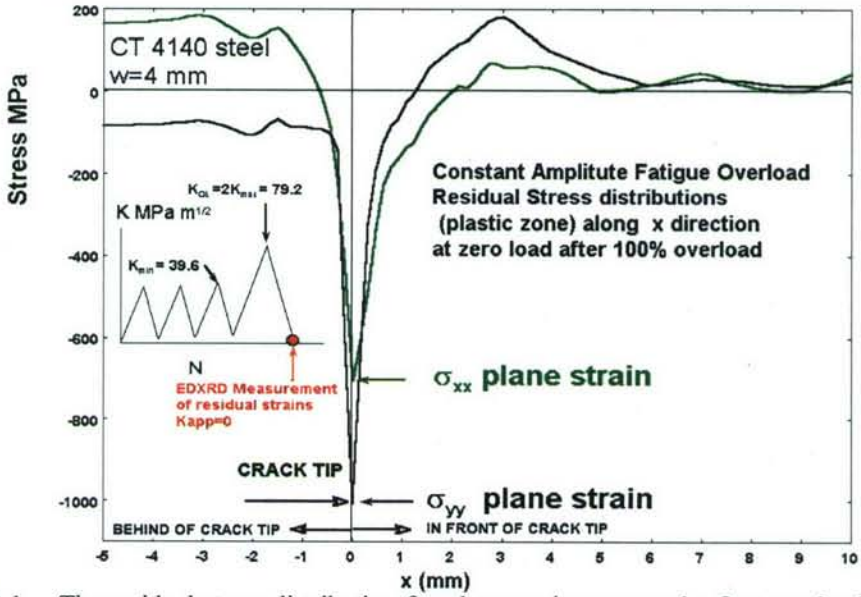

Figure P3.1. The residual stress distribution for plane strain near crack of an overload CT steel specimen. The details of the Fatigue overload experiment and measurement location is shown in the insert

In front of the crack the stress distribution σ_{xx}, outside the plastic zone, shows elastic tensile behavior as expected from the linear fracture mechanics theory despite the fact that the corresponding σ_{xx} goes asymptotically to zero stress from compressive behavior. The experimental value of the overload plastic zone size is $r_{pexperimental}$=3 mm as shown in Figure. P3.1 which is consistent with the theoretical value of $r_{poverload/theoretical}$=2.4 mm. Actually the plastic zone is expected to be larger due to the relaxation

of the stress over the plastic zone region. For elastic perfectly plastic behavior $r_{p\text{-}overload}=2\ r_p$. The maximum compressive stresses near the crack tip for the Plane strain case are σ_{xx}=705MPa, σ_{yy}= 1007 MPa, σ_{zz}=514 MPa. These values suggest a high triaxiality effect for the plane strain case the plastic constraint factor p.c.f=1.56 which is close to Irwin's approximation of 1.68 where as the corresponding p.c.f for plane stress is 1.2.

The stresses behind the crack are approximately σ_{xx}=180 MPa, σ_{yy}=-70 MPa (assuming again plane strain). Near the crack surface the variation of the strain fields are very sharp. Indeed 150 μm away from the crack surface along the y direction the ε_{xx} and ε_{yy} and therefore σ_{xx} and σ_{yy} are exactly zero [2]. This behavior is observed for fatigued, overload-fatigued and fatigued-overload-fatigued deformation. The residual stress distributions well behind the crack tip are independent on the fatigue history, thus suggesting a that major driving force of fatigue crack growth is due to the residual stress distributions in the vicinity of the crack tip [5-7].

Acknowledgements

We wish to acknowledge collaboration with, R. L. Holtz, of the Naval Research Laboratory, and help to choose the parameters, and prepare the fatigue samples in these studies. Moreover, detailed conversations G. Glinka, D. Kujawski, and K. Sadananda are also acknowledged.

References

[1] M. Croft, I. Zakharchenko, Z. Zhong, Y. Gulak, J. Hastings, J. Hu, R. Holtz, M. DaSilva, and T. Tsakalakos, *J. App. Phys.* **92** , (2002) 578 and ref. therein

[2] M. Croft, Z. Zhong, N. Jisrawi,I. Zakharchenko, R.L. Holtz,Y. Gulak, J. Skaritka, T. Fast, K. Sadananda, M. Lakshmipathy, and T. Tsakalakos. Int. J. Fatigue **27**, 1409 (2005)

[3] Paris PC, Erdogan F. A critical analysis of crack propagation laws.
Trans ASME, J Basic Eng 1963;D85:528–34.

[4] see A.H. Noroozi, G. Glinka, S. Lambert International Journal of Fatigue **27**, 1277, (2005)

[5] A. K. Vasudevan, K. Sadananda, G. Glinka, *International Journal of Fatigue*, **23** (2001) S39 and ref. therein.

[6] K. Sadananda, A.K. Vasudevan, R.L. Holtz, and E.U. Lee, *International Journal of Fatigue*, **21** (1999) S233.

[7] M. Lang and G. Marci, *Fatigue Fract. Engng. Mater. Struct.* **22** (1999) 257.

[8] See for example Subra Suresh, *Fatigue of Materials*, (Cambridge University Press, 1998, NY),pp. 305-306.

[9] B. Verma and P. K. Ray, *Bull. Mater. Sci.* **25** (2002) 301.
of Nondestructive Evaluation **17** (1998) 129

[10] M.Croft, Z.Zhong, N.Jisrawi, R.L.Holtz, Y.Gulak, J.Skaritka, T.Fast, K.Sadananda, M.Lakshmipathy, and T.Tsakalakos, manuscript.

[11] AK. Vasudevan, K Sadananda, N.Louat . Mater Sci Eng 1994; A188:1–22.

[12] C. Kittel, *Introduction to Solid-State Physics*, fifth edition, (John Wiley & Sons, 1976, N. Y.) pp. 459-460

[13] G. Glinka, private communication

[14] L. Deck, P. de Groot, Appl. Opt. 33 7334 (1994)